

Biexcitonic gain characteristics in ZnSe-based lasers with binary wells

O. Homburg, P. Michler, R. Heinecke, and J. Gutowski

Institut für Festkörperphysik, Bereich Halbleiteroptik, Universität Bremen, P.O. Box 330440, D-28334 Bremen, Germany

H. Wenisch, M. Behringer, and D. Hommel

Institut für Festkörperphysik, Bereich Halbleiterepitaxie, Universität Bremen, P.O. Box 330440, D-28334 Bremen, Germany

(Received 13 January 1999)

We present systematic spectroscopic studies of the biexcitonic gain and its transition to electron-hole-plasma gain in ZnSe separate-confinement-heterostructure lasers depending on well width, i.e., biexciton binding energy, excitation density, and temperature. The optical gain curves were obtained by means of the variable-stripe-length method under quasistationary conditions. The low-temperature gain spectra are modeled in the framework of a gas of excitons and biexcitons in chemical equilibrium. Sample-dependent redshifts of the gain curves are discussed and compared to the biexcitonic photoluminescence. At elevated temperatures (70–90 K), a steep increase of the laser threshold density accompanied by a strong broadening of the gain curves indicates a change of the gain process towards recombination of a strongly Coulomb-correlated electron-hole-plasma. [S0163-1829(99)08631-2]

I. INTRODUCTION

The understanding of the gain mechanisms in wide-gap II-VI semiconductors as candidates for blue-green laser diodes has attracted much interest in the past. In comparison with conventional III-V semiconductors, where electron-hole-plasma recombination is accepted as the gain mechanism, wide-gap II-VI compounds are characterized by their strong electron-hole correlation. This leads to much larger exciton binding energies, further enhanced in quantum well (QW) structures. Thus, excitonic and biexcitonic features are of key importance for the understanding of the physics leading to gain especially in high-quality low-dimensional II-VI structures at cryogenic temperatures. In the past a couple of exciton-related gain processes have been stated treating the exciton as a stable quasiparticle.^{1–12}

Very recently, a many-particle theory on a microscopic level was presented.¹³ This theory relies on a Green's-function formalism and includes the first-order Coulomb correlations (excitons) self-consistently. Thus, excitonic features are reproduced, and good agreement to the experimental data at elevated temperatures ($T > 100$ K) was achieved.¹⁴ However, the theory is not fully adequate at electron-gas temperatures below 70 K.¹³ At low temperatures, the importance of biexcitons for the formation of gain has been pointed out, e.g., by Kreller *et al.* reporting on lasing due to localized biexcitons in a (Zn,Cd)Se/ZnSe multiple quantum well.^{9,10}

Most widely, the experimental investigations in the past concentrated on (Zn,Cd)Se QW's as active regions in II-VI lasers. These structures are characterized by large inhomogeneous broadening of the $1s$ heavy-hole exciton resonance (X_{hh}) due to well width and additional alloy composition fluctuations of the QW. Thus, localization effects have to be taken into account, eventually leading to gain from localized or extended states, which may change with temperature. This complicates an unambiguous interpretation of the experimental data.

In order to reduce the influence of localization, laser

structures with binary QW's and waveguide/cladding layers consisting of Zn(S,Se)/(Zn,Mg)(S,Se) or (Zn,Mg)(S,Se)/(Zn,Mg)(S,Se) have to be used. Structures involving the latter type of layers can also be operated at higher temperatures due to the better electronic confinement of the carriers. Kozlov *et al.* attributed the gain in an ultrahigh quality 7.5 nm ZnSe/Zn(S,Se)/(Zn,Mg)(S,Se) separate-confinement-heterostructure (SCH) laser at 10 K to an interacting gas of excitons and biexcitons in the absence of localization.^{11,12}

However, to our knowledge, systematic investigations of the gain (especially a line-shape analysis of the gain spectra) in dependence on temperature, well width, excitation density and excitation energy for these binary-QW-based SCH lasers are not yet available. Such studies are inevitable for the development of a consistent microscopic theory covering a large temperature range. Additionally, the gain characteristics of these laser structures are of considerable interest for future applications of semiconductor lasers exhibiting strong Coulomb correlation between the carriers.

In the following, we present photoluminescence (PL) and photoluminescence excitation (PLE) measurements in order to characterize a series of SCH lasers with binary ZnSe QW's of different well widths and, thus, varying biexciton binding energies. Gain curves were obtained by means of the variable-stripe-length (VSL) method¹⁵ under quasistationary conditions. Polarization-dependent fs-pulse pump-and-probe measurements were carried out to get additional insight into the gain mechanism. The temperature-dependent change of the gain process from biexcitonic to Coulomb-correlated electron-hole-plasma recombination is investigated. The low-temperature gain spectra are thoroughly compared to theoretical predictions of the gain due to biexcitonic decay.

The paper is organized as follows. The sample structures and experimental details are described in Sec. II. Sec. III shows the experimental results. At first the samples are characterized at moderate excitation densities, which is followed by the gain data. In Sec. IV the low-temperature data are discussed according to the semiclassical model of a gas of

excitons and biexcitons in chemical equilibrium. Finally, the results are summarized and some conclusions are drawn in Sec. V.

II. SAMPLES AND EXPERIMENTAL DETAILS

In the following the samples are named according to the composition of the waveguide alloy (Quaternary/Ternary) followed by the nominal QW thickness of the active layer. We investigated a 7 nm ZnSe/Zn(S,Se)/(Zn,Mg)(S,Se) SCH laser (sample T7) and a series of ZnSe/(Zn,Mg)(S,Se)/(Zn,Mg)(S,Se) lasers with a QW thickness of 3, 5, and 7 nm (samples Q3, Q5, Q7, respectively). The nominally undoped samples were grown by molecular-beam epitaxy in an EPI 930 twin chamber system. Prior to growth, a 200-nm-thick GaAs buffer layer was deposited on the 2 inch GaAs:Si substrates, which were then transferred *in situ* into the II-VI growth chamber. Elemental sources for Zn, Se, and Mg were used. Sulphur was supplied by a cracker cell being able to change the flux by a valve within a few seconds. At the interfaces of two quaternary compounds with different Mg concentrations, i.e., the interfaces of the waveguides and cladding layers of the samples Q3, Q5, Q7, the temperature of the Mg cell had to be changed by 25°C, corresponding to a factor of two in the beam equivalent pressure. Therefore, the growth was interrupted for 30 min to stabilize the Mg source. During that time, there was no impinging flux on the sample surfaces.

All structures are pseudomorphic with a lattice mismatch of the claddings and the waveguides to the substrate $\Delta a/a$ between 10^{-4} and 10^{-3} . The typical full width at half maximum (FWHM) in high-resolution x-ray diffraction is 30 arc sec. The waveguides have an overall thickness of 170 nm, each cladding layer is 1.2 μm thick. The band-gap energy differences between the wells, waveguides and cladding layers were deduced from PL measurements. The samples Q3, Q5, Q7 with quaternary waveguides are characterized by a total band offset between the QW and the waveguide of about 150–160 meV, with a fraction of 60% in the valence bands. This corresponds to linear optical absorption spectra calculated with the theory approach presented in Ref. 13 and published elsewhere.¹⁶ In contrast to these structures, sample T7 exhibits just a small total band offset between the active layer and the waveguide of approximately 35 meV, whose main part occurs in the valence bands. The total band offsets between the waveguides and the cladding layers amount to 140–160 meV for all samples.

At moderate excitation densities, the samples were excited by a cw Ar⁺-laser-pumped dye-laser beam, which was focussed as a circular spot (diameter $\approx 70 \mu\text{m}$) on the samples. The PL emitted through the sample surface was dispersed by a monochromator and detected by a photomultiplier.

The gain spectra were obtained under quasistationary conditions by means of the VSL method under application of ns laser pulses. The laser system consists of an excimer-laser-pumped dye-laser emitting pulses of 10 ns width. The stripe length was varied between 50 and 300 μm , its width kept fixed to 10 μm . The samples were excited resonantly via the heavy-hole exciton resonance X_{hh} or nonresonantly via the waveguide (barrier). The amplified spontaneous emission

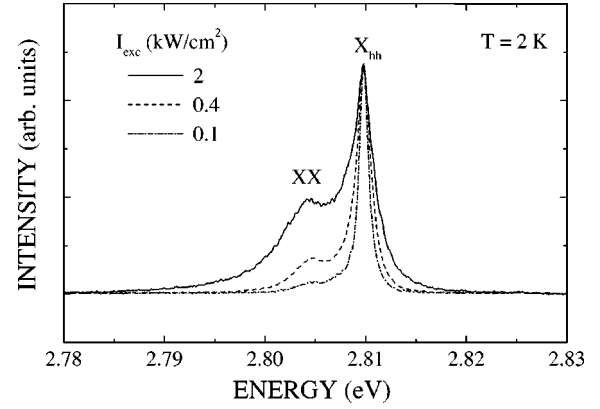


FIG. 1. Normalized PL spectra at different excitation intensities showing the X_{hh} and XX PL lines at 2 K for sample T7, being a typical example for biexcitonic emission. The spectra are normalized to the maximum of the X_{hh} line.

(ASE) emitted from the sample edge was dispersed by a double monochromator and detected by an optical multi-channel analyzer. No polarizer was used. The modal gain $g_{\text{mod}}(E)$ at energy E is extracted from

$$\frac{I_1(E, L_1)}{I_2(E, L_2)} = \frac{\exp[g_{\text{mod}}(E)L_1] - 1}{\exp[g_{\text{mod}}(E)L_2] - 1} \quad (1)$$

with $L_{1,2}$ two different stripe lengths and $I_{1,2}$ the respectively measured intensities of the ASE. The gain spectra presented below were obtained by calculating the gain from up to ten different stripe-length combinations all giving the same gain curves. Thus, inhomogeneities of the stripe or saturation effects are ruled out.

Additionally, polarization-dependent fs-pulse pump-and-probe measurements were carried out. For these experiments, the broad-band beam of a frequency-doubled, mode-locked Ti:sapphire laser, emitting 110 fs pulses at a repetition rate of 82 MHz (spectral width 21 meV), spectrally overlapped both the exciton and biexciton resonances. It was divided into a strong pump and a weak (about 0.1 of the pump) beam, the latter transmitting the sample and being dispersed by a monochromator and detected by a photomultiplier using lock-in technique. For these transmission experiments the opaque GaAs substrate was removed by wet-chemical etching.

III. EXPERIMENTAL RESULTS

A. Characterization of the samples at moderate excitation densities

Exemplarily, Fig. 1 shows typical PL spectra for sample T7 at 2 K, normalized to the X_{hh} PL line intensity. The biexcitonic PL line (henceforth labeled as XX) develops energetically below the X_{hh} emission line and increases super-linearly with the excitation intensity (I_{exc}). The biexcitonic origin of the XX line was proved in polarization dependent four-wave mixing experiments, yielding a biexciton binding energy $E_{\text{XX}}^B = 4.8 \text{ meV}$ for sample T7.¹⁷ The line shape of the X_{hh} emission line is determined by homogeneous and inhomogeneous broadening (Voigt profile). The inhomogeneous linewidth of X_{hh} was extracted in a lineshape analysis yield-

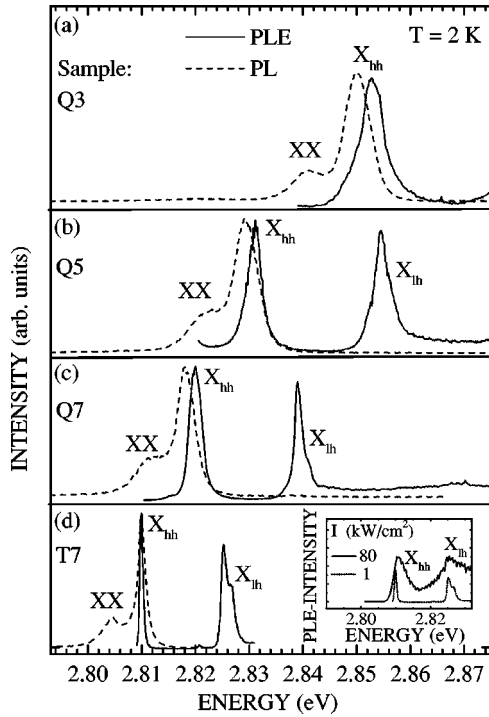


FIG. 2. PL (dashed) and PLE (solid) spectra for the different samples at 2 K and moderate excitation intensities (1 kW/cm^2). The PLE spectra (recorded on the XX line) show the X_{hh} and X_{lh} heavy- and light-hole exciton resonances. Inset: PLE spectra recorded for elevated excitation densities on the XX line (dashed) and ASE maximum (solid) for sample T7.

ing $\Gamma_{inh}^X \approx 0.6 \text{ meV}$, in correspondence with the mainly inhomogeneous linewidth at very low-excitation densities of 1 W/cm^2 . We observe a distinct increase of the homogeneous FWHM of X_{hh} (Γ_{hom}^X) with excitation density in the range from about 0.5 to 2 meV resulting in a stronger overlap of X_{hh} and XX. Γ_{hom}^X is directly related to the dephasing time T_2 of the excitons ($\Gamma_{hom}^X = 2\hbar/T_2$), which strongly decreases with excitation density due to elastic and inelastic scattering processes.¹⁸ We extract dephasing times in the range of some 100 fs up to a few ps, which are of similar magnitude as found elsewhere in the literature.^{18,19}

The PL and PLE spectra of the different samples at 2 K and $I_{exc} = 1 \text{ kW/cm}^2$ are depicted in Fig. 2. The PL spectra show the X_{hh} and XX lines. The PLE spectra were recorded for a detection position on the low-energy tail of the XX line. They exhibit the X_{hh} and $1s$ light-hole exciton (X_{lh}) resonances. At X_{lh} , a doublet structure occurs, which cannot be clearly identified here. However, it is of no importance for the following investigations.

For sample T7, the FWHM of X_{hh} in PLE amounts to 0.7 meV, and no Stokes shift is observed [see Fig. 2(d)]. This allows to study the gain characteristics of an interacting quasi-two-dimensional (2D) system of excitons and biexcitons with negligible localization effects. The samples with quaternary waveguides show blueshifts of the excitonic resonances up to the order of some 10 meV due to quantum confinement [see Figs. 2(a)–2(c)]. This is accompanied by an energetic difference between the excitonic and biexcitonic PL maxima increasing from 5 to 9 meV, which is a rough estimate of the biexciton binding energy. Additionally, the

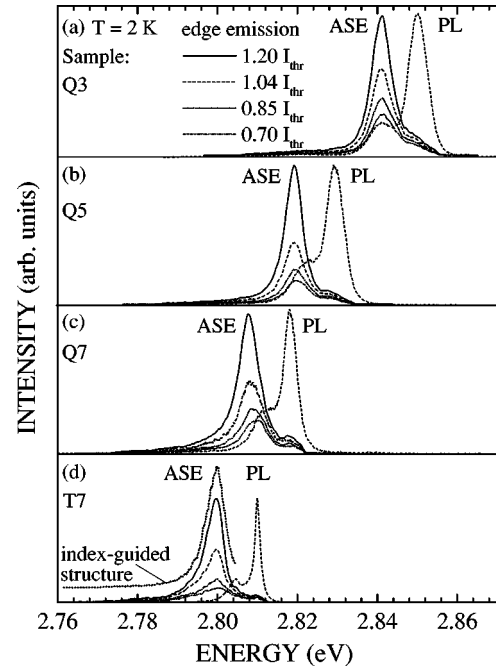


FIG. 3. (a)–(d) PL and edge emission spectra at 2 K for the different samples excited via the waveguide. The evolution of the emission detected from the sample edge is shown from slightly below to slightly above the threshold intensity (I_{thr}) using a stripe length of $220 \mu\text{m}$. (d) Additional ASE spectrum slightly above threshold for an index-guided structure made from sample T7.

samples exhibit FWHM's of X_{hh} in PLE increasing from 2.8 to 5.1 meV, mainly originating from inhomogeneous broadening. They show small Stokes shifts amounting, e.g., to 3 meV for sample Q3. Exemplarily, for sample T7, the inset of Fig. 2(d) depicts the PLE spectrum at high-excitation densities above the laser threshold, which was recorded at the maximum of the ASE emitted from the sample edge in comparison to the PLE spectrum at moderate excitation densities recorded for a detection position on the XX line. We observe an increasing broadening of X_{hh} with excitation density.

In summary, two main features become apparent in the series of samples with decreasing QW thickness: The increased electronic confinement results in a blueshift of the excitonic resonances and an enhanced biexciton binding energy. Additionally, the localization (although weak) is enhanced in the smaller quantum wells due to the increasing influence of well width fluctuations.

B. Gain characteristics of the samples

The threshold carrier densities for the optical net gain (I_{thr}) were estimated from absorption measurements and range from 2 to $5 \times 10^{11} \text{ cm}^{-2}$ for the investigated samples, which is below the nominal Mott density of ZnSe of about $2.5 \times 10^{12} \text{ cm}^{-2}$ at 2 K.²⁰ Sample T7 is characterized by the lowest threshold density of approximately $2.5 \times 10^{11} \text{ cm}^{-2}$. The samples with quaternary waveguides exhibit a slight increase of the threshold density with well width up to $4.4 \times 10^{11} \text{ cm}^{-2}$.

Figure 3 shows, for all samples, in comparison to the PL spectra at $I_{exc} = 1 \text{ kW/cm}^2$, the emission from the sample edge under stripe excitation at waveguide energies and 2 K.

For all samples, the ASE emission from the sample edge evolves spectrally close to the XX line but showing a small sample-dependent redshift. In the sample series with quaternary waveguides this redshift decreases with decreasing well width, and no redshift at all is observed for sample Q3. Strikingly, above threshold the ASE peaks at a nearly constant distance of 9–10 meV below X_{hh} for all samples. On the high-energy side of the ASE emission, a second small peak coincides with the X_{hh} PL line. Obviously, this peak is due to the radiative recombination of excitons.

In order to detect the emission from the sample surface, the samples under stripe excitation were tilted. In this case, the XX line remained spectrally fixed at excitation intensities distinctly above I_{thr} as well as at moderate excitation densities. To rule out that the mostly occurring redshifts of the ASE compared to the XX line are caused by absorption of light in the weakly excited regions at the stripe edges, an index-guided structure of sample T7 was homogeneously excited, exemplarily. Therefore, a laser slab of 10- μm width and 2-mm length was prepared by removing the surrounding ZnSe-based layers of the SCH down to the GaAs substrate by selective etching. The ASE of the homogeneously excited slab (stripe length 220 μm) taken slightly above threshold emerges at the same energy position as in the unprepared sample [see dotted line in Fig. 3(d)]. This finding indicates that the sample-dependent redshift of the ASE maximum compared to the XX line maximum has to be of intrinsic origin in the dense exciton/biexciton system, which is discussed in Sec. IV.

The optical gain spectra were determined by fitting the measured ASE intensity at different stripe lengths on base of Eq. (1). Figure 4 displays the development of the gain at 2 K for sample T7 excited via the waveguide (a) and X_{hh} (b). In the nonresonant case (a), the experimental peak gain coincides with the ASE maximum [compare to Fig. 3(d)]. Like the ASE maximum, the peak gain is slightly redshifted of about 5 meV compared to the maximum of the XX line. The gain curves exhibit small FWHM's of 6–9 meV. The peak gain increases linearly with excitation intensity and its energy position stays constant. The transparency point—the crossover from gain to absorption—exhibits a slight blueshift only. Under resonant excitation (b) the gain maximum is slightly blueshifted when compared to the nonresonant case, and the gain curves possess even smaller FWHM's.

All samples qualitatively show the same gain characteristics. However, in correspondence with the ASE spectra, a diminishing redshift of the peak gain compared to the XX line maximum is observed for decreasing well width, i.e., increasing biexciton binding energy, until complete coincidence of gain and XX line for sample Q3.

Figure 5 gives a complete survey of the dependence of the modal peak gain on excitation intensity and well width for the samples with quaternary waveguides at 2 K. The values were extracted from the various gain curves. The modal peak gain increases linearly with excitation intensity for all samples and reaches values up to 270 cm^{-1} . Higher gain values were not accessible by means of the VSL method due to saturation effects.

For a comparison of the samples the material gain $g(E)$ is more meaningful. It was extracted from

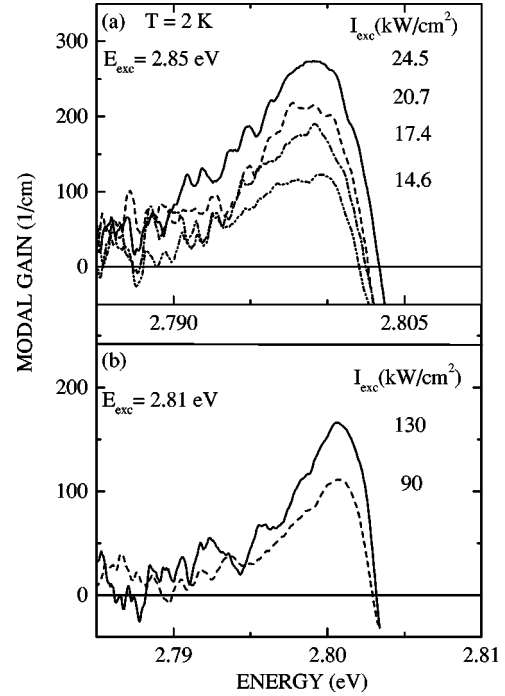


FIG. 4. Experimental gain spectra for sample T7 excited via the waveguide (a) and via X_{hh} (b) at 2 K and different excitation intensities.

$$g_{mod}(E) = \Gamma g(E) - \alpha, \quad (2)$$

with Γ the optical confinement factor. The total loss factor α (caused by scattering of light at crystal defects and by imperfect waveguiding) was neglected, in correspondence with the absence of absorption at the low-energy tail of the gain spectra. The optical confinement factors were calculated to yield 0.032, 0.013, 0.021, 0.029 for the samples T7, Q3, Q5, Q7, respectively. Thus, high material gains of about $1 \times 10^4 \text{ cm}^{-1}$ are obtained, with sample Q3 providing the highest value of $1.5 \times 10^4 \text{ cm}^{-1}$.

To get even more insight into the gain mechanism, polarization-dependent fs-pulse pump-and-probe measurements were carried out for sample T7 at 2 K. Figure 6 shows the differential-transmission spectra in the vicinity of X_{hh} and XX without time delay between the pump and probe

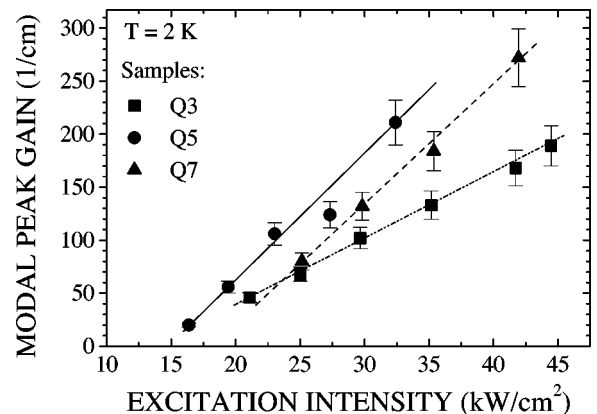


FIG. 5. Excitation intensity dependence of the peak gain at 2 K for the samples with quaternary waveguides excited via the waveguide.

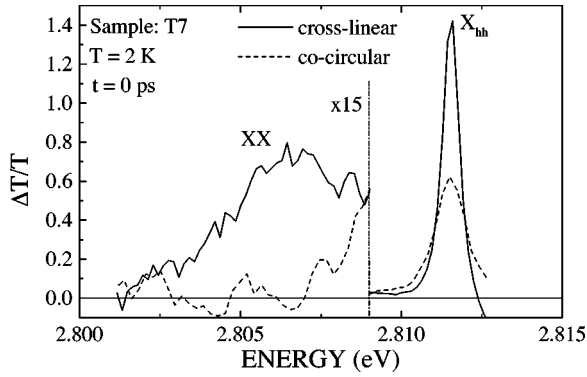


FIG. 6. Differential-transmission spectra for sample T7 at 2 K excited resonantly by fs pulses slightly above the laser threshold using cross-linearly (solid) and co-circularly (dashed) polarized pump and probe pulses.

pulse for two different polarization arrangements, namely cross-linearly and co-circularly polarized light at an excitation density slightly above the laser threshold. Under both polarization configurations induced transmission is observed at the spectral position of X_{hh} . Under excitation with cross-linearly polarized light, induced transmission is additionally observed at the spectral position of the biexcitonic resonance. Since in the linear optical regime no absorption was found at this spectral position, this corresponds to real optical gain. In contrast, no gain is observed for co-circularly polarized light for which biexciton creation is forbidden. These findings are a clear signature of biexcitonic contributions to the gain.¹² However, if the differential-transmission spectra are compared to the gain curves which were obtained under quasistationary conditions (see Fig. 4), the latter will exhibit a redshift, which is discussed in Sec. IV in detail.

In Fig. 7(a), the temperature dependence of the laser threshold intensity for the samples Q3 and Q7 is exemplarily depicted. For both samples the curves can be divided into three temperature regions exhibiting distinguished characteristics. At low temperatures the threshold intensity stays nearly constant. This is followed by a more or less pronounced decrease at 50 K for both samples. This is probably due to the thermal activation of carriers, e.g., previously bound to impurities but now also feeding the gain process. Between 70 and 90 K—when the thermal energy is close to the biexciton binding energy—a steep increase of the threshold intensity indicates the dissociation of biexcitons and the change of the gain process towards Coulomb-correlated electron-hole-plasma recombination. For sample Q7, this increase is very abrupt between 70 and 80 K. This corresponds to thermal energies $k_B T = 6-7$ meV (compare to $E_{XX}^B \approx 5 \pm 1$ meV given in Sec. III A). Sample Q3 shows a more gradual increase of the threshold intensity at higher temperatures from 80 to 120 K, corresponding to thermal energies $k_B T = 7-10$ meV (compare to $E_{XX}^B \approx 8 \pm 1$ meV).

At more elevated temperatures, the threshold intensity exponentially increases with temperature, which is most commonly observed for lasing by electron-hole-plasma recombination.^{14,21}

In addition, distinct changes of the gain curves are observed at elevated temperatures. In Fig. 7(b), the gain spectra are plotted at 100 K for sample Q3, exemplarily. The gain

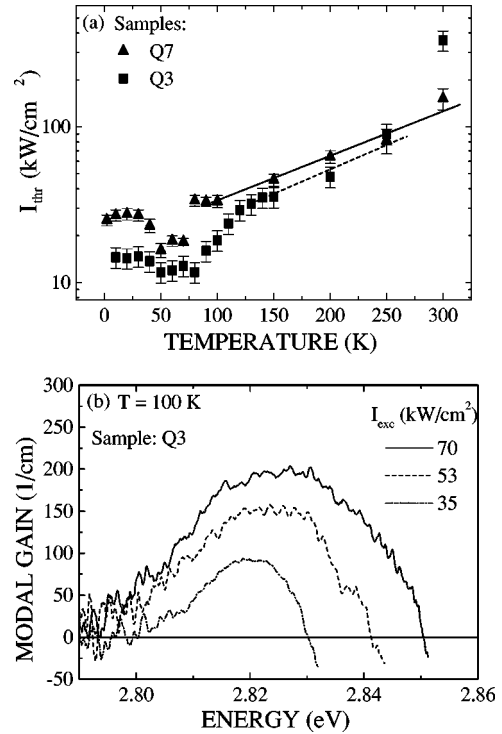


FIG. 7. (a) Temperature dependence of the threshold intensity for the samples Q3 (squares) and Q7 (triangles) excited via the waveguide. (b) Corresponding gain curves for sample Q3 at 100 K under different excitation intensities.

curves are strongly broadened. The FWHM at $I_{exc} = 70$ kW/cm² amounts to 38 meV. A large blueshift of the transparency point with excitation intensity is detected. This is accompanied by a small blueshift of the peak gain. At higher temperatures these effects are even more pronounced. All these characteristics are in accordance with the features of gain due to recombination of a Coulomb-correlated electron-hole-plasma, which obviously takes over at elevated temperatures. Corresponding calculations on the basis of a first-principles theory presented in Ref. 13 are published elsewhere.¹⁶ Therefore, in the following discussion we concentrate on the low-temperature gain characteristics.

IV. DISCUSSION

Because of their high quality, the investigated samples allow to study even small changes of the gain curves in detail. The experimental data give clear evidence that the radiative decay of biexcitons is the prominent gain process at low temperatures. A most appropriate theoretical approach including biexcitonic contributions to the gain would be a many-particle theory on a microscopic level, where excitonic and biexcitonic correlations are self-consistently accounted for. However, such a theory is, at the moment, far from being established and might be a challenge for future advanced theory development.

The model we apply here relies on a widely-used semiclassical two-level system consisting of a gas of excitons and biexcitons in chemical equilibrium.²²⁻²⁵ Since the samples were excited by laser pulses of 10 ns width, being large compared to the radiative lifetimes of about 100 ps of excitons and biexcitons in ZnSe-based QW structures, and to the

relaxation times on a ps time-scale, the exciton (n_X) and biexciton (n_{XX}) densities can well be assumed to be in a steady state. According to this classical treatment, biexcitons can be formed in a collision process of two excitons, whereas in the reverse process a biexciton may dissociate into two excitons. The particle densities n_X and n_{XX} of the exciton/biexciton gas in chemical equilibrium with effective temperature T_{eff} are related by a mass action law²²⁻²⁴

$$\frac{n_X^2}{n_{XX}} = n^*, \quad (3)$$

$$n^* = \frac{d_X^2}{d_{XX}} \left(\frac{1}{2\pi\hbar^2} \frac{m_X^2}{m_{XX}} \right) (k_B T_{eff}) \exp\left(\frac{-E_{XX}^B}{k_B T_{eff}} \right), \quad (4)$$

where d_i , m_i , $i=X,XX$ denote the degeneracies and masses of the exciton and biexciton, respectively, and n^* the equilibrium constant.

Accordingly, optical gain develops in the exciton/biexciton system due to population inversion between the X_{hh} and XX states depending on the momentum \mathbf{k} . The radiative decay of a biexciton into an exciton and a photon follows the reaction



Assuming a \mathbf{k} -independent dipole matrix element and a Boltzmann distribution of the kinetic energies, the two-dimensional (2D) gain coefficient $g(E)$ for the biexciton gain process ($XX \leftrightarrow X_{hh}$) is simply related to the spontaneous emission rate $P_{sp}(\hbar\omega)$ by²⁶

$$g(E) \sim \left[1 - \eta \exp\left(-\frac{E_{XX} - E_X - E}{k_B T_{eff}} \right) \right] P_{sp}(\hbar\omega), \quad (5)$$

$$\text{with } \eta = \frac{m_{XX} d_{XX} n_X}{m_X d_X n_{XX}}, \quad (6)$$

denoting the excitation-induced reabsorption ($X_{hh} \rightarrow XX$) depending on the ratio n_X/n_{XX} , which may lead to redshifts of the gain curves compared to the spontaneous emission spectra.²⁶ E_X and E_{XX} denote the energies of the exciton and biexciton, respectively. With the spontaneous emission rate $P_{sp}(\hbar\omega)$ for 2D biexcitonic decay follows in analogy to 3D biexcitonic decay²⁴

$$g(E) = C \frac{n_{XX}}{T_{eff}} \left[1 - \eta \exp\left(-\frac{E_{XX} - E_X - E}{k_B T_{eff}} \right) \right] \times \theta(E_{XX} - E_X - E) \exp\left(-\frac{E_{XX} - E_X - E}{k_B T_{eff}} \right). \quad (7)$$

C is a constant including the dipole matrix element and $\theta(E_{XX} - E_X - E)$ denotes the biexcitonic 2D density of states.

In ZnSe QW structures four degenerate X_{hh} resonances ($s_e = \pm 1/2$, $j_h = \pm 3/2$), two optically allowed excitons and two dark states, have to be considered. Since our experi-

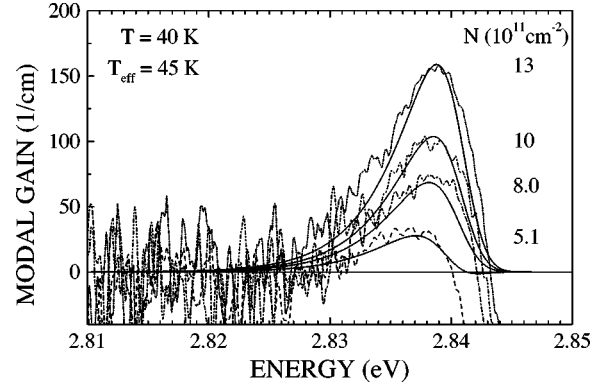


FIG. 8. Experimental (dashed) and corresponding calculated (solid) gain spectra for sample Q3 with increasing carrier densities (N) at $T=40$ K and $T_{eff}=45$ K.

ments were carried out under quasistationary conditions, scattering and spin-flip processes of the carriers occur very effectively on a short time-scale, so that all four degenerate X_{hh} states are eventually equally occupied ($d_X=4$). One nondegenerate biexciton ground state ($J_{XX}=0$, $d_{XX}=1$) is accounted for. The translational masses of the biexciton and exciton are taken as follows: $m_{XX}=2m_X$, $m_X=1.26m_0$.²⁷

As already mentioned in Sec. III B, for sample Q3, which is characterized by the largest biexciton binding energy, the ASE and the gain developed in spectral coincidence with the XX line [see Fig. 3(a)]. For the experimental regime of high-carrier densities ($>5 \times 10^{11} \text{ cm}^{-2}$) and slightly elevated temperatures (40 K) the influence of the anyway weak localization becomes negligible, and the application of the above model is reasonably justified. Figure 8 shows the experimental and calculated gain spectra for sample Q3 at 40 K for different excitation densities. For the calculations, the values of $E_{XX}^B=8$ meV, $E_{X_{hh}}=2.849$ eV and $\Gamma_{inh}^X=5$ meV were deduced from PL and PLE measurements, so that the effective temperature T_{eff} remained the only fitting parameter apart from the normalization constant C . The best overall agreement between the calculated and experimental gain spectra was obtained with T_{eff} between 40 and 50 K. The calculated gain curves show a very good agreement with the experimental data. Especially, at high-excitation densities (upper three spectra), the model reproduces the linear increase and constant energy position of the peak gain with excitation density as observed for the other samples as well (see Sec. III B). Additionally, in correspondence with the experiment, the calculated gain curves exhibit just a slight blueshift on the high-energy side at high-excitation densities. However, the upper three calculated spectra do not show the crossover from gain to absorption. This is a consequence of accounting for only one transition ($XX \leftrightarrow X_{hh}$) and neglecting transitions at higher energies, especially the X_{hh} absorption ($0 \rightarrow X_{hh}$). Thus, at high-excitation densities population inversion between XX and X_{hh} occurs for all energies E , and no absorption is observable in the calculated gain spectra ($\eta < 1$).

However, if the energy separation between X_{hh} and XX (E_{XX}^B) is small, the influence of the excitonic absorption ($0 \rightarrow X_{hh}$) on the high-energy side of the biexcitonic gain cannot be neglected, i.e., the biexcitonic gain might be overruled by excitonic absorption leading to a redshift of the gain

maximum. Indeed, the sample-dependent redshifts of the gain curves compared to the XX line, which were experimentally observed with decreasing biexciton binding energy, might be explained by the increasing influence of X_{hh} absorption. Considering the strong linewidth broadening of X_{hh} on the order of some meV at elevated excitation densities, which is comparable to $E_{XX}^B=4.8$ meV for sample T7 (see Sec. III A), the exciton and biexciton resonances are not clearly separated and X_{hh} absorption is expected to play an important role.

Whereas the gain curves that were obtained for sample T7 under quasistationary conditions exhibit these redshifts (see Fig. 4), the gain in the differential-transmission spectra more closely coincides with the XX line (see Fig. 6). Under fs-pulse excitation without pump-probe delay, the gain in the coherent polarization regime is probed, and scattering processes (dephasing) can be neglected. Thus, the gain is due to cold biexcitons without excess energy that were coherently created by the broadband pump pulse in a two-photon absorption process as stated in Ref. 12.

Most probably even more important, Kozlov *et al.*¹² demonstrated a very complicated and distinguished gain dynamics in dependence on time, carrier density and polarization configuration. Especially, they observed *optical gain and absorption across the biexcitonic resonance*, which they attributed to the interplay between coherent and incoherent effects. In our experiments under quasistationary conditions, we extracted the modal gain from the ASE from the sample edge perpendicular to the exciting laser pulse. In this case, the exciton/biexciton gas undergoes a manyfold of scattering processes and reaches the fully incoherent regime, in contrast to the fs-pulse experiments at $t=0$. Thus, the spectral position of the quasistationary net modal gain has not necessarily to coincide with the gain in the coherent polarization regime.

V. SUMMARY AND CONCLUSIONS

The low-temperature data are interpreted in the framework of a gas of excitons and biexcitons in chemical equilibrium. We successfully modeled the main gain features on base of a semiclassical two-level system of the involved excitations. At low temperatures and high-excitation densities, the peak gain increases linearly, and its energy position remains nearly constant. The transparency point exhibits a slight blueshift only. With increasing effective carrier temperatures the theoretical gain curves shift to the red in correspondence with the observed redshift of the peak gain under waveguide excitation when compared to resonant excitation. A mostly occurring redshift of the peak gain compared to the XX line maximum was, to its main parts, attributed to exciton absorption superimposed to the biexciton transition in particular for those samples exhibiting a small energy separation of the exciton and biexciton resonance. At elevated temperatures a change of the gain mechanism to Coulomb-correlated electron-hole-plasma recombination was demonstrated.

For a better understanding of the gain characteristics especially for the samples exhibiting low-biexciton binding energies, a more sophisticated theoretical approach would be inevitable, in which the exciton/biexciton system is treated on a microscopic level including dephasing effects. This is well beyond the scope of this paper.

ACKNOWLEDGMENTS

We thank M. F. Pereira for stimulating discussions. The sample epitaxy was supported by the Deutsche Forschungsgemeinschaft (Grant No. Ho 1388/8).

-
- ¹C. B enoit   la Guillaume, J. M. Debever, and F. Salvan, *Phys. Rev.* **177**, 567 (1969).
- ²H. Haug and S. Koch, *Phys. Status Solidi B* **82**, 531 (1977).
- ³C. Klingshirn and H. Haug, *Phys. Rep.* **70**, 315 (1981).
- ⁴J. Ding, M. Hagerott, T. Ishihara, H. Jeon, and A. V. Nurmikko, *Phys. Rev. B* **47**, 10 528 (1993).
- ⁵Y. Kawakami, I. Hauksson, H. Stewart, J. Simpson, I. Galbraith, K. A. Prior, and B. C. Cavenett, *Phys. Rev. B* **48**, 11 994 (1993).
- ⁶J. Gutowski, A. Diessel, U. Neukirch, D. Weckendrup, T. Behr, B. Jobst, and D. Hommel, *Phys. Status Solidi B* **187**, 423 (1995).
- ⁷L. Calcagnile, D. Greco, G. Coli, R. Cingolani, M. Lomascolo, M. Di Dio, L. Sorba, and A. Franciosi, *Superlattices Microstruct.* **21**, 119 (1997).
- ⁸L. Calcagnile, D. Cannoletta, R. Cingolani, M. Lomascolo, M. Di Dio, L. Vanzetti, L. Sorba, and A. Franciosi, *Phys. Rev. B* **55**, 13 413 (1997).
- ⁹F. Kreller, M. Lowisch, J. Puls, and F. Henneberger, *Phys. Rev. Lett.* **75**, 2420 (1995).
- ¹⁰F. Kreller, J. Puls, and F. Henneberger, *Appl. Phys. Lett.* **69**, 2406 (1996).
- ¹¹V. Kozlov, P. Kelkar, A. V. Nurmikko, C.-C. Chu, D. C. Grillo, J. Han, C. G. Hua, and R. L. Gunshor, *Phys. Rev. B* **53**, 10 837 (1996).
- ¹²V. Kozlov, P. Kelkar, A. V. Nurmikko, C.-C. Chu, D. C. Grillo, J. Han, C. G. Hua, and R. L. Gunshor, *Phys. Rev. B* **54**, 13 932 (1996).
- ¹³M. F. Pereira, Jr. and K. Henneberger, *Phys. Rev. B* **58**, 2064 (1998).
- ¹⁴P. Michler, M. Vehse, J. Gutowski, M. Behringer, D. Hommel, M. F. Pereira, Jr., and K. Henneberger, *Phys. Rev. B* **58**, 2055 (1998).
- ¹⁵K. L. Shaklee, R. E. Nahory, and R. F. Leheny, *J. Lumin.* **7**, 284 (1973).
- ¹⁶P. Michler, M. F. Pereira Jr., O. Homburg, L. Nerger, J. Gutowski, H. Wensch, and D. Hommel, *Proc. SPIE* (to be published).
- ¹⁷G. Bartels, A. Stahl, V. M. Axt, B. Haase, U. Neukirch, and J. Gutowski, *Phys. Rev. Lett.* **81**, 5880 (1998).
- ¹⁸H. Nickolaus, F. Henneberger, and A. Schultzen, in *Semiconductor Heteroepitaxy Growth, Characterization and Device Applications*, edited by B. Gil, R.-L. Aulombard (World Scientific, Singapore, 1995), p. 147.
- ¹⁹D. Weckendrup, M. Saschek, U. Neukirch, and J. Gutowski, *J. Appl. Phys.* **77**, 4145 (1995).
- ²⁰S. Schmitt-Rink, D. S. Chemla, and D. A. B. Miller, *Adv. Phys.* **38**, 89 (1989).

- ²¹J. Singh, *Semiconductor Optoelectronics, Physics and Technology* (McGraw-Hill, Singapore, 1995).
- ²²P. L. Gourley and J. P. Wolfe, Phys. Rev. B **20**, 3319 (1979).
- ²³J. C. Kim, D. R. Wake, and J. P. Wolfe, Phys. Rev. B **50**, 15 099 (1994).
- ²⁴J. Collet and T. Amand, Phys. Rev. B **33**, 4129 (1986).
- ²⁵J. M. Hvam, Solid State Commun. **26**, 987 (1978).
- ²⁶T. Kushida and T. Moriya, Phys. Status Solidi B **72**, 385 (1975).
- ²⁷S. Lankes, J. Appl. Phys. **80**, 4049 (1996).